Journal of Dynamic Behavior of Materials
https://doi.org/10.1007/s40870-022-00340-z

RESEARCH PAPER

Dynamic Behavior and Impact Tolerance of Elastomeric Foams Subjected to Multiple Impact Conditions

B. Koohbor[1,2] · G. Youssef[3] · K. Z. Uddin[1] · Y. Kokash[3]

Received: 7 February 2022 / Accepted: 9 May 2022
© Society for Experimental Mechanics, Inc 2022

Abstract
Hyperelastic foams are an ideal class of impact mitigating materials in applications where more than a single impact loading event may exist. However, methods and protocols used to characterize impact tolerance in hyperelastic foams subjected to multiple impact conditions are limited and provide insufficient information about the impact load-bearing efficacy of the material. In this work, we present a comprehensive experimental approach that allows for investigating the dynamic behavior and impact tolerance of a novel elastomeric polyurea foam. The proposed approach includes conventional experimental techniques, e.g., impact force analyses, supplemented by full-field strain measurements and the evaluation of strain-dependent Poisson's ratio of the foam as additional metrics that enable a detailed study of the evolution of the macroscopic dynamic behavior of the foam in response to multiple impacts with variable impact energies. The experimental measurements are coupled with mesoscale finite element analyses and post-deformation microstructural observations. Results obtained herein indicate the possibility of internal damage formation as the primary source of the slight decrease in impact mitigation efficacy. Specifically, the highly stretched polyurea cell walls in the foam are identified as the source of microscopic, permanent damage. Despite the significant damage developed during the multi-impact loading, the foam retains an effective level of overall impact energy mitigation capacity.

Keywords Impact loading · Polyurea · Elastomeric foams · Digital image correlations · Multiscale analysis

Introduction

The persistent challenges of developing effective impact mitigating structures can be resolved using elastomeric foams, potentially sustaining single and multiple impact loadings [1–3]. Cellular solids have been proven effective in such dynamic loading scenarios in different applications, ranging from packaging and sports gears, irrespective of the attributes of microcellular structure, whether it is random foams (scholastic) or ordered honeycombs (lattice) [4, 5]. Impact mitigating structures (e.g., protective paddings used in sports gears) undergo several low-velocity impacts during relatively short durations (i.e., game time). Therefore, they must consistently perform at the same or comparable protective levels with high efficacy by withstanding the incoming force pulses and absorbing the impact energy. The challenge resides in damage accumulation in the bulk material and the microcellular structures, which is exaggerated in rigid foams but can be wholly circumvented in their elastomeric counterparts. The former is suitable for single impact scenarios and has been integrated broadly into the shipping and packaging industry [2]. The scientific and technological potential of the elastomeric foams serves as the motivation for the research leading to this report.

A prime example of elastomeric foams is the emergent polyurea foam, recently reported to inherit some of the superior mechanical properties of its base material. Polyurea, a thermoset elastomer, exhibits superior engineering attributes, chiefly the shock and impact tolerance, making it an ideal material candidate for several civilian and military applications over several decades of strain rates [6–9]. Of specific interest is the cryogenic glass transition

✉ B. Koohbor
koohbor@rowan.edu

1 Department of Mechanical Engineering, Rowan University, 201 Mullica Hill Rd, Glassboro, NJ 08028, USA

2 Advanced Materials & Manufacturing Institute, Rowan University, Glassboro, NJ 08028, USA

3 Experimental Mechanics Laboratory, Mechanical Engineering Department, San Diego State University, San Diego, CA 92182, USA

Published online: 08 June 2022

temperature, indicating polyurea is well within the rubbery regime at ambient temperatures with significant extensibility, providing large strain energy potential [10]. Several studies investigated the thermomechanical behavior by measuring the acoustic and dynamic responses as a function of temperature, demonstrating the interdependence of the creep strain and the moduli on changes in temperature [11, 12]. The addition of microcellular structure to polyurea (i.e., foamed polyurea) resulted in hyper-viscoelastic elastomeric stochastic solid capable of effectively sustaining low-velocity impacts without incurring severe permanent damage. Two research groups independently foamed polyurea using drastically different methods in the recent literature. Ramirez et al. [13–15] used a heat-activated chemical foaming agent to achieve several densities, ranging from ~ 100 to 300 kg/m^3. Alternatively, Reed et al. [16, 17] reported a self-foaming process relying on the intrinsic reaction between isocyanate and water, resulting in large entrapped volumes of carbon dioxide gases when violently mixing the constituents. The heat-free version of polyurea foam (i.e., after Reed et al.) was cured and dehydrated at room temperature before being submitted to quasi-static and dynamic loadings [16, 18]. The density of the second polyurea foam version was limited compared to their heat-foamed counterparts, suggesting a manufacturing challenge for ultralow density elastomeric polyurea foam; a topic of future research due to its practical importance. It is worth noting that the novelty of polyurea foam reported by Reed et al. stems from the hierarchal microstructure and self-reinforcement with polyurea microspheres nucleating during the mixing process via precipitation polymerization [19]. The outcomes culminated in targeting the mitigation of two biomechanical impact scenarios, including football helmets [18, 20] and density-graded orthotics [21].

In their seminal work on polymeric cellular solids, Ashby and Gibson cataloged the ideal and realistic mechanistic response of rigid and elastomeric foams [1], including the potential mechanisms leading to plastic failure. Generally, the quasi-static stress–strain behavior of microcellular polymers is exploited for the mechanical characteristics of the foam, including elastic, plateau, and densification regions, to forecast the dynamic behavior [1, 22, 23]. The initial elastic region is associated with limited and reversible deformation, resulting in the instantaneous stiffness of the foam as the interplay between the mechanical properties of the base material (entrapped in the cell edges and walls) and the geometrical attributes of the cellular structure [1]. The plateau region, bounded between the outset of the elastic region and onset of the terminal densification region, defines the energy-absorbing ability of foams, where extended plateau (i.e., large deformation at nearly constant stress) implies higher energy absorption abilities. Finally, the densification region is where the interplay between the base material and deformed cellular structure dominates the response, resulting in maximum efficiency. The latter, being a dynamic property, was shown to forecast using the results of the quasi-static response with a certain degree of certainty [24–26]. That is, the quasi-static predictions are not a substitute for dynamic testing, as discussed in [27], where other time-dependent phenomena take precedence, including viscoelasticity, inertial effects, and working fluid contributions. In the plateau and densification regions, several deformation mechanisms are activated to contribute to the overall efficacy of the foam, including elastic and plastic buckling of cell edges and walls, elastic and plastic kinking of the cell walls, yielding, and plastic deformation of the base material. These damage mechanisms collectively limit the utility of rigid foams in repetitive impact loadings. However, their effects can be demoted in elastomeric foams, marking them an ideal engineering material candidate for such common low-velocity impact scenarios (e.g., walking, running, or other sports events).

As mentioned above, emergent polyurea foams have undergone extensive experimental quasi-static and dynamic investigations with strain rates ranging from ~ 0.05 s^{-1} to > 200 s^{-1} [16, 28]. It was reported that the hierarchical, self-reinforced microcellular structure of polyurea foams plays a vital role in their mechanical performance irrespective of the strain rate. Regardless of the density, polyurea foams, similar to those investigated herein, exemplified multifaceted microcellular structures, consisting of large spherical unit cells with ~ 4.5–7.6% perforations due to the self-limiting chemical reaction [16], surrounded by closed spherical cells. Such microstructure lends polyurea foams into the conventional classification (i.e., mechanical response with positive Poisson's ratio); however, recent work by the authors demonstrated that impact low-density polyurea samples could result in mild auxetic conversion due to plastic deformation [29]. This is remarkable since such impact-converted auxetic polyurea foams persisted in effectively mitigating low-velocity impacts, even after several impacts with different energies [29]. While it was stipulated that the localized plastic deformation might play a role in the conversion phenomena, the interrelationship between the plastic deformation and the nearly auxetic conversion was neither investigated nor revealed; hence, the focus of the research leading to this paper.

The objective of this paper is to characterize the dynamic behavior and impact tolerance of a novel polyurea foam subjected to multiple impacts with controlled impact energies. Specifically, the foam samples are subjected to a sequential, multi-level impact scenario with an ascending-descending impact energy input. The impact tolerance behavior of the foam is examined by tracking various metrics, including the evolution of load-bearing and Poisson's ratio. Experimental studies are supplemented by a multiscale finite element

analysis that allows for studying local damage evolution in the impacted foam test piece. The outcomes of this work point to the possibility of impact-induced cellular-scale damage, potentially affecting the impact tolerance of the examined foam.

Materials and Methods

Sample Preparation

Low-density, elastomeric polyurea foam (with a nominal density of 110 kg/m^3) was utilized in this work due to its pronounced hyperelastic behavior. Polyurea foam slabs were prepared based on the recipe detailed in Refs. [16, 17, 19] by violently mixing an amine (oligomeric diamine, Versalink P1000, AirProduct Inc.), isocyanate (modified Methylene Diphenyl Diisocyanate, Isonate 143 L, DOW Industrial), and deionized water. Upon curing and dehydration, cubic samples with a nominal 18 mm edge size were punched out of the slabs. These sample dimensions were selected to ensure that the extracted specimens are sufficiently large to represent the macroscale mechanical response of the foam [30]. The microstructural characteristics of the foam were examined using a scanning electron microscope (SEM, FEI, Quanta 450), where Fig. 1 shows a representative SEM micrograph from an unloaded sample. The average cell size and cell wall thickness of the investigated polyurea foam samples were characterized using image analysis of the SEM micrographs. The cell wall thickness distribution was determined using an image-based approach (performed in open-source software ImageJ) in which the size of a straight line that connects each cell exterior to its nearest neighbors is measured first. Next, the same approach is applied to a randomly selected large collection of cells in the SEM micrographs. The measured values are then processed to find the mean (average size) and standard deviation (size variability) of the parameter of interest, i.e., cell wall thickness. Accordingly, the average cell size and cell wall thickness were determined as 302.3 ± 91.3 µm and 82.9 ± 28.1 µm, respectively, which are in good agreement with previous results [30]. The significantly high coefficient of variation (standard deviation-to-mean ratio) in the cell wall thickness indicates the highly nonuniform distribution of cell wall thickness, which is reflected in the visual, qualitative evaluation of the SEM image in Fig. 1. The geometrical attributes of the microcellular structure were used as input to the finite element analyses discussed in the forthcoming sections.

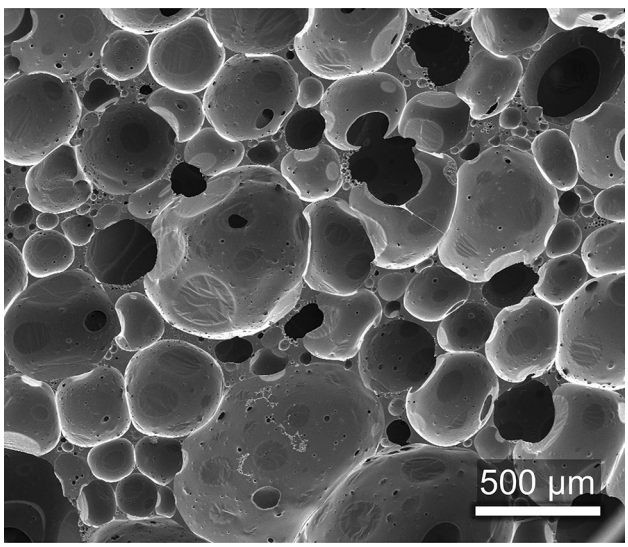

Fig. 1 SEM micrograph of the examined low-density polyurea foam, showing the microcellular size distribution of 302.3 ± 91.3 µm and its ubiquitous spherical attribute

The compressive stress–strain response of the foam under quasi-static loading conditions was examined for reference. For quasi-static characterizations, foam samples were tested under a constant compression rate of 5 mm/min (equivalent to a 4.6×10^{-3} s^{-1} nominal strain rate). Stress–strain and Poisson's ratio evolution of the foam under quasi-static conditions were extracted based on the experimental protocols described later.

Impact Testing and Force Measurement

The extracted foam cubes were subjected to multiple low-velocity impacts with controlled impact energy input based on the drop height, i.e., controlling the potential energy. Seven consecutive direct impacts were exerted on each foam sample using a 723 g flat impactor dropped from specific heights (Fig. 2). Accordingly, the impact energies of 1.77, 3.55, 5.32, and 7.09 J were determined for the drop heights of 250, 500, 750, and 1000 mm, respectively, representing impact velocities ranging between 2.2 and 4.2 m/s. The drop weight experiment and the calculation of input energy reported in [18] were modified and adopted herein to accommodate the repetitive loading scenarios. As shown in Fig. 2a, the impact scenarios were designed in an ascending-descending manner to analyze the impact energy-dependent mechanical response of the foam, as discussed in the forthcoming sections. Notably, a four-minute rest time was constituted between the successive impact events to allow for strain recovery in the sample, storing images captured during the impact test, and adjusting the drop weight to the next position. The transmitted force-time histories were recorded using a sensor located at the bottom of the foam sample (Fig. 2a) as part of the drop tower setup. Data reproducibility in the impact tests was confirmed by conducting the same impact scenario on multiple foam samples. Due to the sample-to-sample microstructural variations, the exact values of

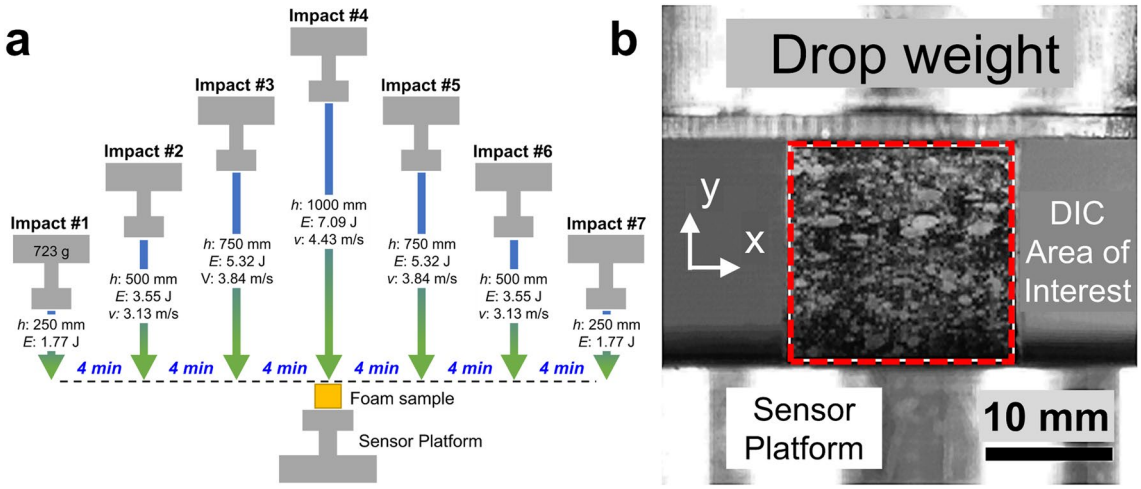

Fig. 2 **a** Schematic representation of the multiple impact loading conditions applied on the foam sample. **b** A close-up view of the foam sample showing its camera-facing speckled surface used for digital image correlation

the measured quantities of interest varied, while the trends (discussed in later sections) were confirmed repeatable.

High-Speed Photography and Image Correlation

The impact force measurements were supplemented by an image-based quantitative analysis of the sample deformation by digital image correlation (DIC). To this end, a high-speed camera (Photron FASTCAM SA1.1) was used to capture images from the front surface of the sample at an image acquisition rate of 40,000 fps. For DIC purposes, the surface of interest, i.e., the front surface, must be coated with high contrast and random pattern. However, due to the large and repeated impact deformation conditions applied, a conventional spray paint coating of the front surface of the sample was not practical. Instead, the porous surface features of the foam samples (e.g., Fig. 1) were used as a natural speckle pattern for DIC analyses [31]. To further improve the image contrast, the natural light-yellow surface color of the sample was lightly coated with a thin layer of alcohol-based black paint, leaving the surfaces of the open cells to serve as the speckle pattern effectively. The DIC area of interest in the sample is shown in Fig. 2b.

Images acquired by the high-speed camera were analyzed in the commercial digital image correlation software Vic-2D (Correlated Solutions, Inc., SC, USA) with subset and step sizes of 23 pixels (6.08 mm) and 8 pixels (2.12 mm), respectively. An incremental correlation approach was used to enable full correlation at large deformation conditions. The in-plane strain fields were calculated using a Gaussian filter with a window size of 5 data points applied to the raw displacement fields. The step and strain filter sizes utilized in this work made it possible to measure full-field strain with a virtual strain gauge size of 10.6 mm (calculated as the product of step size × strain filter), which is roughly triple the representative volume element (RVE) size of the examined foam [30]. In-plane strain components, ε_{xx} and ε_{yy}, were used to determine the Poisson's ratio. Accordingly, the strain-dependent Poisson's ratio of the samples was determined using the instantaneous (tangent) definition of this parameter, as $\nu = -\mathrm{d}\in_{xx}/\mathrm{d}\in_{yy}$. The instantaneous definition of Poisson's ratio was used over the total (secant) formulation, as the former has been proven more effective in capturing the true values of this parameter, especially for low-density foams and those that tend to show auxetic response [31].

A similar procedure was followed to identify the strain-dependent Poisson's ratio of the foam under quasi-static conditions. The logarithmic (true) definition of strain was used throughout this report, including for the characterization of local (micro) and global (macro) deformation behaviors in both quasi-static and dynamic loading conditions.

Impact Tolerance Metrics

Various metrics were used to characterize the impact tolerance of the examined foam material. Comparing the peak force values recorded in each of the seven successive impact events was used as the first criterion. The peak force was used to assess the impact tolerance and the variation of the load-bearing capacity of the foam. Furthermore, since the multiple impact scenarios involved hitting the sample at the same height (i.e., energy level) twice, the change of the peak force resulting from impacting the foam at the same energy level is a byproduct metric, implying the effect of the accumulated damage. For example, the difference in the peak forces measured from the first and seventh impacts, i.e., at 1.77 J, indicates the internal damage that might have

occurred within the cell walls, which might alter the impact performance of the foam.

The corresponding evolution of the maximum compressive strain developed in the foam (quantified by DIC) was another metric for the characterization of impact tolerance. Finally, the strain-dependent Poisson's ratio of the foam, resulting from submitting the samples to repetitive impact events, has been determined and used as a practical metric for studying the load-bearing behavior of the foam. Poisson's ratio was previously used as a primary metric for quantifying the foam materials' tendency to distort [31, 32]. The strain-dependent Poisson's ratio in low-density foams has been correlated with strain localization and significant local shear deformation, leading to damage initiation and accumulation over successive loading events [32]. As such, the evolution of the apparent Poisson's ratio (deduced from the full-field deformation of the front surface) was considered a factor determining the impact-induced damage and impact tolerance of the examined foam. The aforementioned impact tolerance criteria were complemented by microscopic imaging of the foam sample after the loading cycle.

Multiscale Finite Element Analysis

Multiscale finite element analysis was conducted to study the correlations between strain fields developed at macro and micro scales. An idealized two-dimensional array of circular cells with dimensions equal to the average cell size of the examined foam (i.e., 302 µm) in a polyurea matrix was created as the domain of interest (see Fig. 3a). The spacing between the circular cells in this RVE was designed to be equal to the average cell wall thickness of the utilized foam, i.e., 83 µm. Overall dimensions of the RVE model were chosen as 3.5 × 3.9 mm to ensure that the domain size is large enough to encompass enough cells to represent the macroscale behavior of the foam [30]. Material properties assigned to the solid sections of the model were obtained for solid polyurea under quasi-static tension (~ 0.013 s^{-1} strain rate), as shown in Fig. 3b. The tensile failure strain (logarithmic) of the examined polyurea was determined as ~ 1.9. The experimental stress–strain values were fitted with an Ogden-4th order model for ease of application in the FE solver. The utility of a quasi-static analysis in lieu of a dynamic counterpart stems from a twofold rationale. First, polyurea is well within the rubbery regime when tested at room temperature under low and moderate strain rates since its glass transition temperature is nearly − 50 °C. Hence, the hyperelastic response dominates and eclipses the viscoelastic contributions. Second, the primary objective of developing this model is to elucidate the geometrical changes in the idealized unit cells as a function of the magnitude of the force. Such changes can be considered a sole function of the latter in light of the mechanical behavior of polyurea within

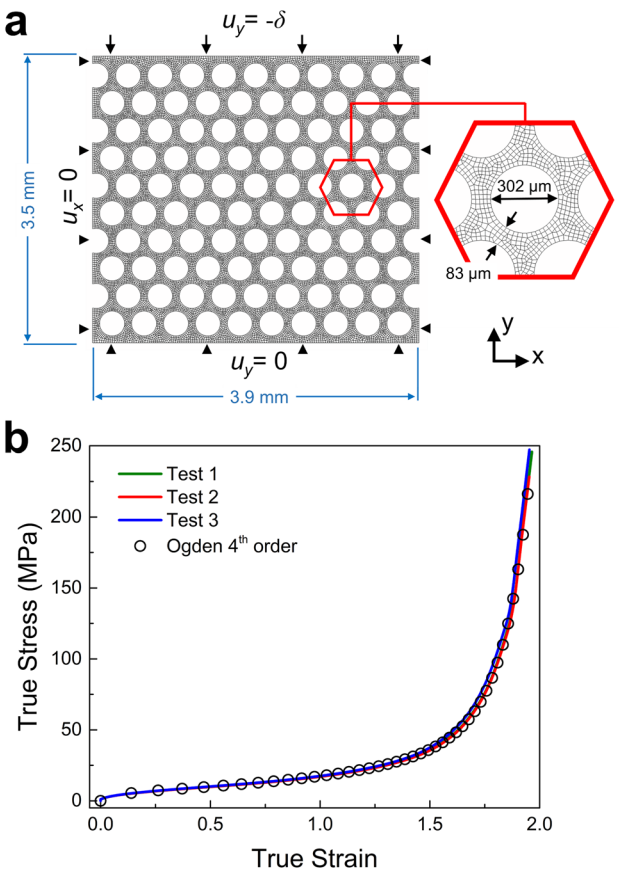

Fig. 3 **a** Finite element model representing a simplified RVE of the polyurea foam examined in this work. The cell diameter and cell-wall thickness sizes were designed to be equal to the average values of the two parameters determined experimentally for the actual foam samples. **b** Experimental and fitted true stress–strain curves of the base polyurea used as input to the FE model. Three tests were conducted to ensure the repeatability of the results

the rubbery regime. In other words, the quasi-static finite model can elucidate the geometrical changes in the unit cell, as discussed later, without any loss of generality.

Finite element simulations were performed in the commercial package Abaqus®. The FE model was meshed with 30,319 CPE4H (4-node bilinear plane strain quadrilateral) elements, selected after an iterative mesh sensitivity analysis to identify the mesh size that does not influence the deformation results. Self-contact interactions were implemented in the model by assigning an internal friction coefficient of 0.2 inside the cell walls [33]. Note that an internal friction coefficient is required to ensure no mutual penetration between the nodes and elements of opposing cell walls in a fully compressed foam. Considering that the FE analysis was used to determine the local strains developed in cells walls before densification and complete cell closure (as further discussed in the following), the utilized coefficient of friction is merely for

numerical convenience. As shown in Fig. 3a, the two vertical and the horizontal bottom edges of the model were fixed in x- and y-directions, respectively. The near-zero Poisson's ratio of the foam (measured experimentally, as discussed later) was applied to the model by fully constraining the lateral displacement of the vertical domain boundaries. A downward displacement of $\delta = 1.8$ mm was applied on the top horizontal boundary of the model to represent the axial compression imposed during experiments. For simplicity, the rate-dependent response of the solid polyurea was suppressed in this model. To characterize the correlations between local (micro) and global (macro) strains, the evolution of local strain fields developed over cell walls were extracted and compared with the global strain applied on the model.

Results and Discussion

Quasi-static Mechanical Response

The quasi-static stress–strain response and the corresponding strain-dependent evolution of Poisson's ratio are plotted in Fig. 4. The mechanical response of the foam is typical of those for other elastomeric foams, indicating an initial high apparent stiffness, followed by a slope change that correlates with the elastic buckling of the cell walls at microscopic scales [34]. At global strains of ca. 0.3, another increase in the slope of the curve is observed. This final change of slope in the stress–strain response of the foam marks the onset of global densification, occurring due to the excessive compression and closure of the cells in the foam [1].

The evolution of the Poisson's ratio during deformation was also characterized using the approach presented in previous publications [19, 28]. As shown in Fig. 4b, the instantaneous Poisson's ratio exemplifies an initial high value of ~0.15. Once the deformation history reaches large compressive strains, the Poisson's ratio decreases to a minimum value of ~0.05 achieved at a global compressive strain of 0.3. The Poisson's ratio tends to increase following the onset of global densification. The final increase observed in the Poisson's ratio originates from the local closure of the cells in the foam, leading to a reduction in the foam's ability to accommodate the applied deformation through cell buckling and other micromechanics phenomena. Instead, the behavior of the compressed, densified foam converges to the mechanical response of its solid constituent (i.e., polyurea), where the Poisson's values reach those of incompressible solids [35]. Nonetheless, the Poisson's effect in the examined foam indicates (1) a strain-dependent behavior and (2) values close to those of compressible solids (i.e., $\nu = 0$), at least before the onset of global densification.

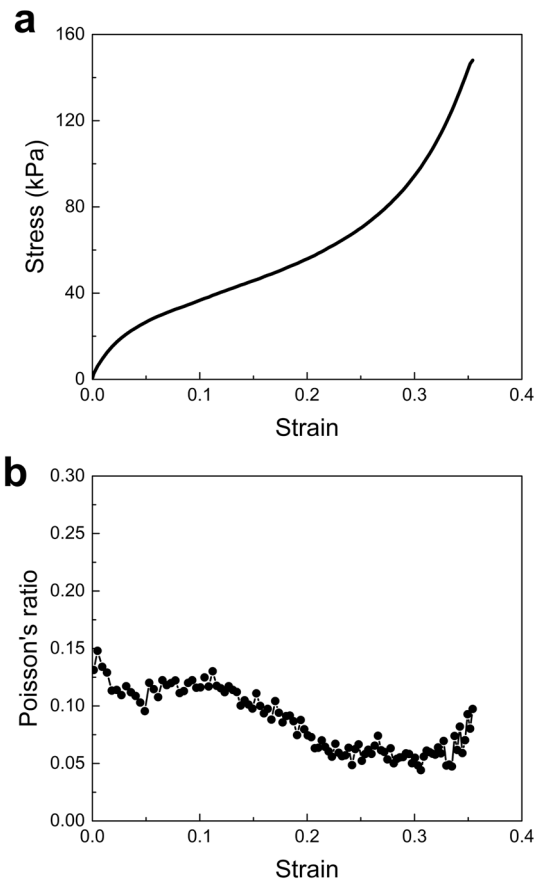

Fig. 4 **a** Stress–strain and **b** Poisson's ratio evolution of the examined foam under quasi-static (4.6×10^{-3} s^{-1}) compression. Strain values in this figure are logarithmic (true) values. The oscillations in **b** are due to numerical derivation of the raw stain data obtained from DIC analyses

Multiscale Strain Analysis

The stress–strain and Poisson's effect characterized under quasi-static conditions point to the significance of micromechanics evolutions that govern the macroscale behavior of the foam. To shed light on some of the more significant micromechanics developments, a simplified foam model was used as the input to a finite element analysis (see Fig. 3). Figure 5a shows snapshots of the deformed FE model extracted at different global strains. The evolution of the first principal strain in the vicinity of a single cell (located at the center of the domain) is also shown in Fig. 5b. The first principal strain was used as the parameter of interest because it represents the maximum local tensile strain developed at a point irrespective of the orientation. Therefore, this parameter can be used to correlate the maximum tensile local strain, as a critical metric for the possibility of microscale damage, to the global compressive strain applied on the foam test piece.

Deformation patterns developed in the RVE show a uniform compression up to global strains of ~0.03.

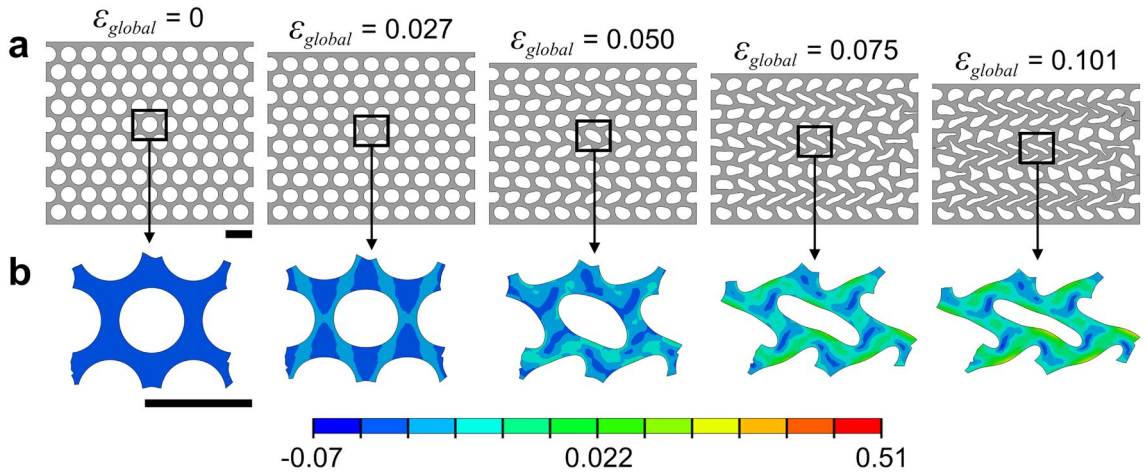

Fig. 5 Snapshots extracted from the FE model to show the evolution of deformation at **a** RVE and **b** single cell length scales. The contour maps in **b** represent the evolution of first principal strain, as a metric for the evolution of local tensile strains generated over elastically buckled cell walls. Scale bars = 500 µm

Interestingly, this global strain falls within the initial high-slope region of the global stress–strain curve shown earlier in Fig. 4a. At higher global strains, the buckling of the vertical cell walls is evident at the RVE scale and also from the asymmetric deformation of the single cell in Fig. 5b. The cell buckling behavior continues at higher global strains by developing non-uniform deformation patterns at RVE and single-cell scales. Besides the well-known buckling-dominated deformation response of the cells illustrated in this figure, a more interesting observation is the formation of highly stretched local regions within the cell walls in response to the applied compressive deformation. To quantify such local strain anomalies, the variation of the aforementioned local maximum principal strain has been plotted in Fig. 6 with respect to the global strains applied on the RVE model. Note that the global compressive strain has been plotted as positive values in this figure, and both strain metrics are in logarithmic (true) values. In addition, the local strains are extracted from a 'hot spot', i.e., a critical region located on the cell wall near the interior of the cell.

A linear trend approximates the evolution of the local vs. global strain up to a global strain of ca. 0.05. Then, the linear trend abruptly changes into a nonlinear correlation with a significantly higher slope, indicating a sudden shift of the microscale deformation response from a stable, uniform compression to an unstable, highly non-uniform buckling mode. Another significant outcome of this analysis is the comparison between the numerical values of the local and global strains. To better reflect on this comparison, a simple '*strain ratio*' metric has been defined as the ratio between the local maximum principal strain and the global compressive strain. The evolution of the strain ratio is also shown in Fig. 6. In line with the local deformation mechanism shift

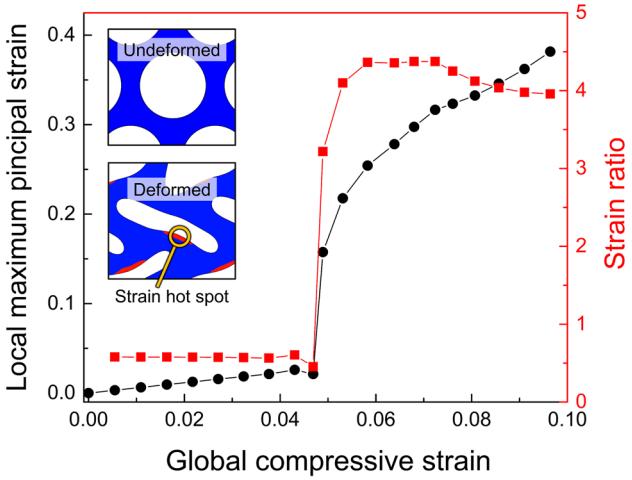

Fig. 6 Variation of local maximum principal strain (as a measure for the local tensile strain developed on cell walls) plotted with respect to global compressive strain. The 'strain ratio' parameter as the ratio between the two strain values is also plotted. Local maximum strain is extracted from the strain 'hot spot' marked on the figure inset

discussed above, the strain ratio shows a sudden increase upon the initiation of the cell wall buckling mode. Values greater than 4 are obtained for this metric, indicating the substantial differences between the local and global strains in low-density foams subjected to compressive forces. Consistent observations were made by Koohbor et al. [36] in an experimental study that characterized the local and global strains in rigid foams subjected to high strain rate loading conditions. The major difference between the observations made in the current study and those reported in Koohbor et al. [36] is the reversible mechanical behavior of the flexible foams examined here, which directly correlates with the

capability of the base polymer (i.e., polyurea) in the present study to withstand large tensile deformations.

Before delving into further details and the use of such strain ratios in dynamic loading conditions, it is worth mentioning that the strain ratios identified herein can be utilized to predict the maximum compressive strains achievable in polyurea foams before the solid polyurea cell walls start to fail. Accordingly, assuming (1) a perfectly ordered cell distribution with uniform circular cells and cell wall sizes and (2) an invariable strain ratio of 4 that remains valid at large strain conditions, one could estimate a maximum compressive strain of 1.9/4 = 0.475 (based on a tensile failure strain of 1.9 for polyurea and a strain ratio of 4) as the maximum strain tolerable by the foam before any internal damage. This estimated strain was used as a guideline to design the impact conditions applied to the foam samples, as discussed in the forthcoming sections.

In practice, the assumption of a perfectly ordered cell structure is not realistic. Instead, the cell structure of polyurea foam, as exemplified by the SEM micrograph (Fig. 1), contains a variety of cells shapes and sizes with a wide range of cell wall thicknesses. In such conditions, the probability of achieving large local strains on thinner cell walls increases, leading one to assume that the cell scale damage is even more probable in actual foam structures. Another noteworthy point is the role of high strain rate conditions. Assuming that similar strain ratios will hold at high strain rate loading conditions, due to the strain rate-induced reduction of the failure strain in polyurea [37, 38], the probability of internal damage formation increases. Superimposed to the latter is the role of internal pressure build-up, especially for closed or semi-closed cell foams subjected to high strain impact loadings [28, 39]. The combination of the two aforementioned factors leads to even higher strain ratios (as shown by Koohbor et al. [36] for closed-cell rigid polyurethane foams) and an increased propensity of elastomeric foams to internal damage formation when subjected to impact loading conditions, as discussed in detail in the forthcoming sections.

Impact Force History

The deformation state generated in the foam is induced by submitting the samples to repetitive impact loadings at different energies by adjusting the drop height. The force-time histories of consecutively impacting polyurea foam at different energies are reported in Fig. 7, demonstrating the resiliency of the foam to repeated impacts. The difference in the peak force between the first and seventh (both done at 1.77 J) is merely 80 N, representing a 10% increase after submitting the same foam sample to cumulative impact energy of ca. 28.3 J. Such difference in the force amplitude increased when comparing the earlier and later impacts at the same

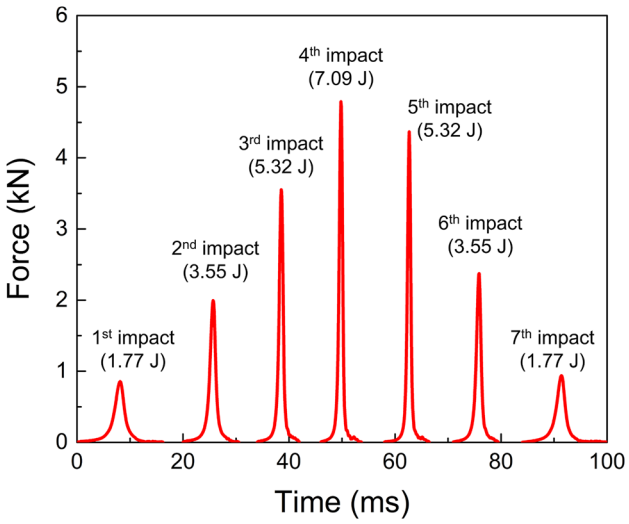

Fig. 7 Variation of impact force, recorded at the bottom of the same impacted foam plug, for seven consecutive impact loadings

energy. For example, the peak force difference for impacting the foam at 3.55 J was 380 N when comparing force-time history from the second and sixth impacts. The peak difference reached a maximum upon impacting the foam at 5.32 J (i.e., third and fifth impacts), reporting an increase of 810 N or ~ 22%. The evolution in the difference peak force as the number of impacts increases is attributed to three underlying mechanisms. First, the reduction in the impact energy resembled in the impact events after the fourth impact, mirroring the energy of those before, resulting in submitting the foam to lower overall forces, allowing the engagement of force dissipation and time broadening mechanisms discussed previously. Second, the imposed resting time to accommodate experimental logistics implies that the last impact was at least 24 min after the first event, allowing the foam extended relaxation times. That is, continuous relaxation processes instigated ongoing recovery as the time elapsed between the first and last impacts. Finally, the severity of the higher energy impacts (e.g., 7.09 J impact) induced internal damage (discussed later), resulting in strain-softening and strengthening mechanisms that directly benefited the reported force-time history. The evidence for the strain-softening, where the strain for the seventh impact is higher than the initial impact at the same energy, is reported and discussed in the next section.

Macroscale Strain Response and Poisson's Ratio Evolution

Figure 8 shows the temporal evolution of normal in-plane strain components, i.e., ε_{yy} and ε_{xx}, developed in the foam. These strain components were calculated as the spatial average of the strain fields that were extracted from the

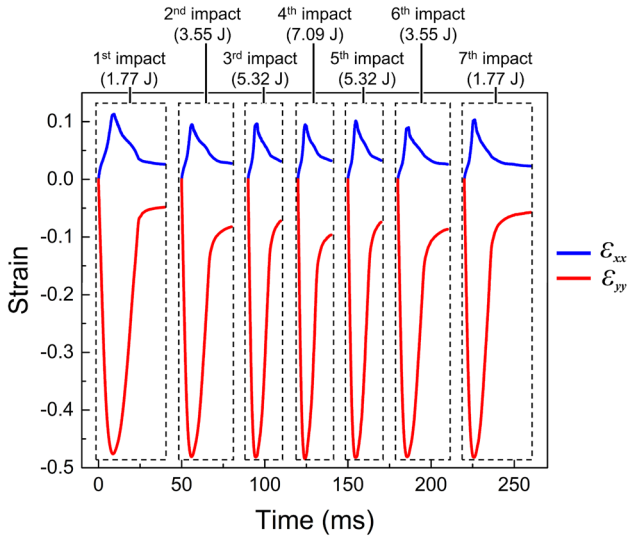

Fig. 8 Variation of axial, ε_{yy}, and transverse, ε_{xx}, strain components developed in the foam sample subjected to seven consecutive impact loadings

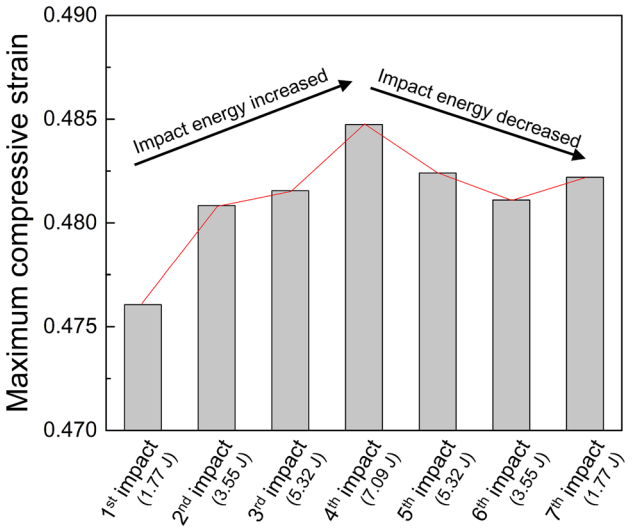

Fig. 9 Variation of maximum axial (compressive) strain recorded in the sample after multiple impact events

high-speed images using DIC [28]. Since the camera was offline during the 4-min resting period between two successive impacts, each DIC analysis was performed while taking the reference (zero-strain) condition as the first image captured for each impact event. Nonetheless, the evolution of the strain components follows similar patterns, i.e., an initial increase in value, indicative of the loading half-cycle, followed by a strain decrease during the unloading phase. However, the strain components are vastly different in value due to the compressible nature of the foam, which attributes to a small Poisson's ratio. The latter is indicated by the significantly smaller transverse strain, ε_{xx}, compared with the axial strain, ε_{yy}. Although not characterized in detail in this work, the non-zero strains at the end of each loading event are due to the viscoelastic nature of the foam that prevents immediate, full recovery of the foam to its original state [18].

A significant observation in the strain response is the nearly unchanged maximum axial strains developed in the foam in response to a quadrupled impact energy, even though the impacted force exerted on the sample varies consistently with the impact energy. This maximum compressive strain is close to the theoretical threshold (i.e., 0.475) determined in "Multiscale Strain Analysis" section. A comparison between the maximum compressive axial strains developed in the sample in response to seven successive impact events (with 4-min rest periods) is shown in Fig. 9. The maximum compressive strain during the first four impact events (i.e., the ascending energy impact cases) follows an increasing trend, suggesting an apparent energy-dependent deformation response. Such an increase mirrors the recorded force evolution shown in Fig. 7. On the other hand, the maximum strain values do not follow a monotonic pattern during the descending energy impacts scenarios. In particular, the maximum compressive strain developed in the same sample during the first and the last impacts show a slight difference, although the input energy for the two impact cases is equal. The difference is manifested by a relatively larger development of maximum compressive strain in the foam. Considering the same impact energy magnitudes applied during the 1st and the 7th impact loading, the relatively larger maximum compressive strain can be an indicator of irreversible microstructural variations in the sample in response to repeated impact.

In addition to the strain analysis, the evolution of the Poisson effect due to multiple impacts was also quantified. Figure 10a shows the strain-dependent Poisson's ratio evolving during successive seven impacts. The general trends are similar to those obtained for quasi-static conditions (Fig. 4b), showing a higher value at small strains. At increasing strains, the Poisson's ratio decreases to a local minimum. The rise in Poisson's ratio at strains > 0.25 is related to the onset of global densification, where the foam tends to behave like an incompressible solid. A qualitative comparison of the curves suggests an overall decreasing trend in the Poisson's ratio in response to multiple impacts. This decreasing trend is further analyzed in Fig. 10b by plotting the evolution of Poisson's ratio at two representative strains (global strains of 0.1 and 0.2) and in response to the seven impact events applied. The Poisson's ratio values in Fig. 10b show a rapid decrease, reaching a plateau. The decrease in the Poisson's ratio can be related to the foam's partial loss of resistance to compressive deformation, which is a consequence of the microstructural changes discussed next.

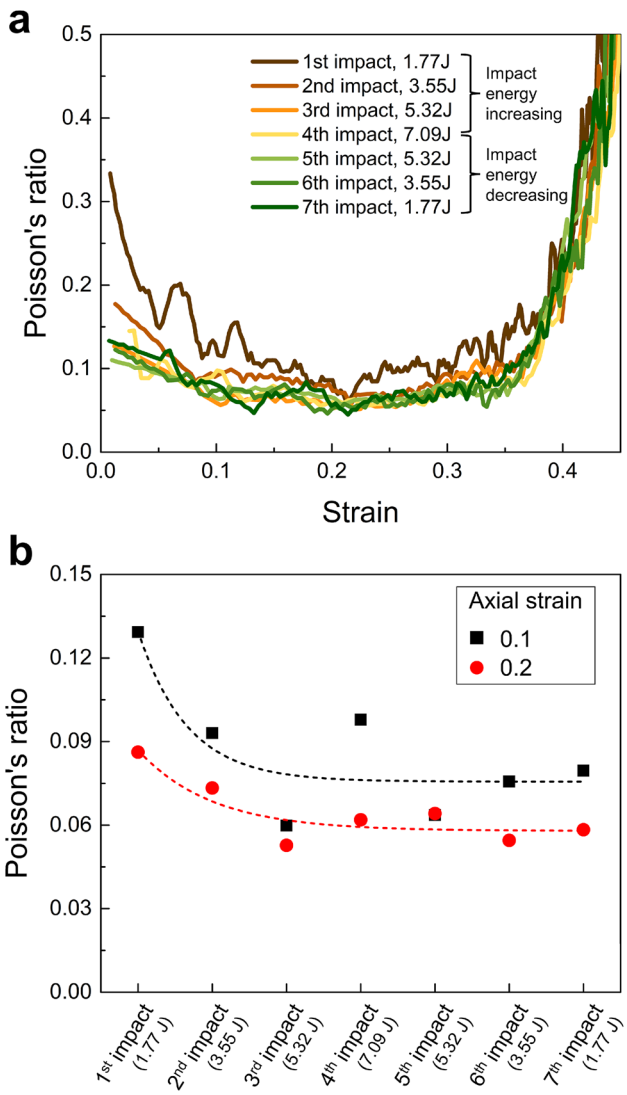

Fig. 10 **a** Variation of Poisson's ratio with respect to the applied compressive strain in multiple impact loading conditions. **b** Evolution of Poisson's ratio in the impacted foam extracted at two representative strains of 0.1 and 0.2

The loss of resistance to compressive deformation is also elucidated in Fig. 11 by full-field strain maps that show the distribution of local ε_{yy} fields at a global strain of 0.3, i.e., just before the onset of global densification. A qualitative comparison between the cases with the same impact energy (e.g., 1st and 7th impacts) clearly shows the evolution of larger compressive strains and higher degrees of strain heterogeneity developed in the impacted foam. The increased strain heterogeneity indicates the presence of localized deformation fields (in the form of internal shear bands, not possible to observe at macroscales) that lead to local damage formation and a tendency to develop a near auxetic behavior [32].

Internal Damage

In spite of the flexible nature of the examined foam, the experimental measurement of peak force, maximum strain, and Poisson's ratios collectively point to the possibility of internal damage formed in the foam in response to the multiple impacts applied. Evidence for such internal damage evolution after multiple impacts can be observed in the SEM micrographs in Fig. 12. This figure shows the microstructure of the foam plug, illustrated earlier in Fig. 1, after exposure to seven successive impacts. The cell structure of the impacted foam shows clear differences compared with its original state. First, the initially spherical cell geometry has been altered to an elliptical cell geometry that is indicative of an irreversible residual deformation. As shown by the two magnified subsets, the cell walls also show evidence for severe buckling (Fig. 12b). The buckling is also observed on the exterior of the cells in the form of wrinkles and overfolds illustrated in a close-up view in Fig. 12c.

In all, despite the nominal hyperelastic nature of the polyurea foam sample used in this work, the multiple impact loadings applied have caused irreversible microstructural changes that lead to a partial loss of integrity and impact load-bearing efficacy of the foam. However, as shown by several criteria used for evaluating the impact tolerance of the test piece, the polyurea foam studied herein shows acceptable performance for applications where multiple high-intensity impacts are to be exerted on the foam structure. Last but not least, the evidence for the aforementioned irreversible microstructural damage seems to saturate after the first few impacts, giving the foam the ability to retain its impact loading resistance. While beyond the scope of the present study, the long-term use and impact tolerance

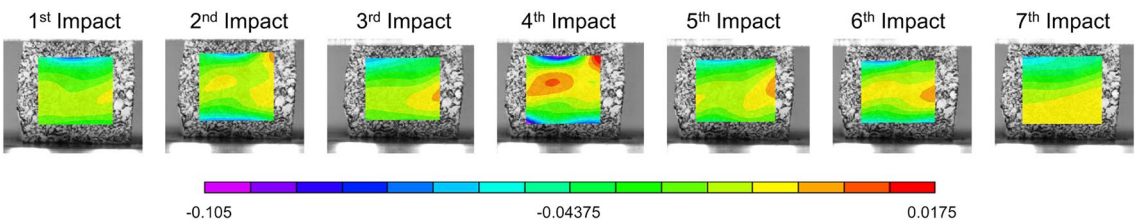

Fig. 11 Contour maps showing ε_{yy} strain fields at a global strain of 0.3 in the seven consecutive impact loadings

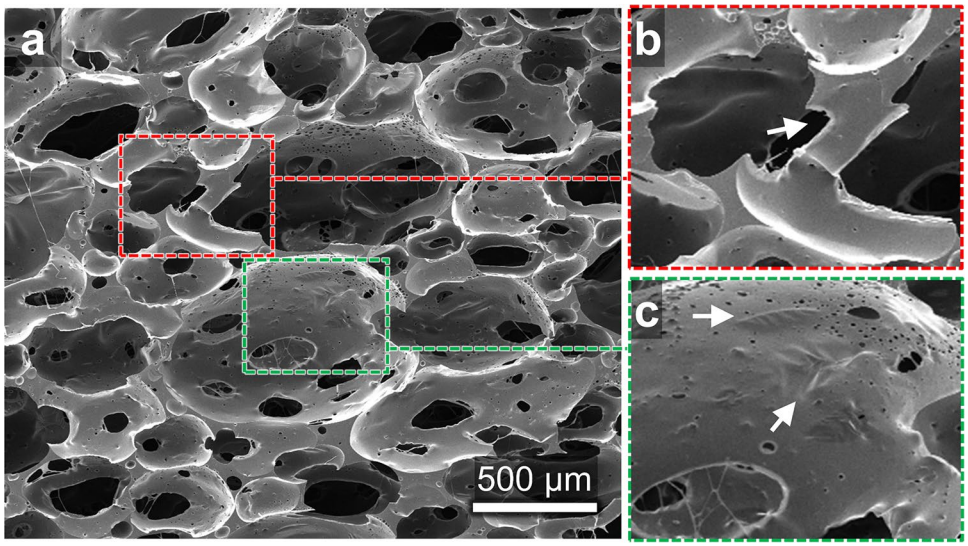

Fig. 12 **a** SEM micrograph of the foam subjected to seven impact events, showing evidence of **b** cell wall buckling and **c** wrinkles

efficacy of the examined polyurea foams is an interesting topic for future research. In general, polyurea foams represent an ideal material candidate to mitigate single and repetitive biomechanical impact scenarios (i.e., low-velocity impacts) in several applications, including orthotics, sports protective paddings, and helmets. The resilience of this foam translates into potentially transformative performance to reduce risks of trauma and concussion.

Summary

A hybrid experimental-modeling approach investigated the efficacy of a novel hyperelastic polyurea foam subjected to impact loading conditions. A single polyurea foam plug was subjected to a multiple-impact scenario wherein the impact energy was adjusted to follow an ascending-descending trend, thus subjecting the sample to controlled and repeatable impacts. The dynamic behavior and load-bearing capacity of the foam were characterized using various experimental measurements. The capability of the foam in resisting impact deformation was characterized by measuring the impact force and maximum strains developed in the foam piece. Experimental results demonstrated that the foam sample partially loses its ability to resist impact loading due to permanent deformation and damage developed at cellular scales. The internal damage was also associated with the strain-dependent Poisson's ratio variation in the foam. A mesoscale finite element analysis investigated the variations in macroscopic properties, revealing the possible micromechanics phenomena, most notably in the form of highly stretched polyurea cell walls, leading to irreversible deformation and damage at microscales. Evidence for such irreversible mechanisms was revealed by SEM imaging of the post-deformation microstructure. Despite the irreversible microstructural variations that occurred during the multi-impact loading of the sample, the examined polyurea foam was proven effectively capable of retaining its overall impact load-bearing capacity.

Acknowledgements This material is based upon work supported by the National Science Foundation under Grant No. 2035660 (B.K.) and Grant No. 2035663 (G.Y.). B.K. acknowledges the Advanced Materials and Manufacturing Institute (AMMI) at Rowan University for the financial support. We acknowledge the use of equipment at SDSU's Electron Microscopy Facility acquired by NSF grant DBI-0959908.

Data Availability Data will be made available upon request.

Declarations

Conflict of interest The authors declare no conflict of interest (financial or non-financial).

References

1. Ashby MF, Gibson LJ (1999) Cellular solids: structure and properties, 2nd ed. Cambridge University Press
2. Mills N (2007) Polymer foams handbook: engineering and biomechanics applications and design guide, 1st ed. Butterworth-Heinemann
3. Youssef G (2021) Applied mechanics of polymers: properties, processing, and behavior. Elsevier
4. Rahman O, Uddin KZ, Muthulingam J, Youssef G, Shen C, Koohbor B (2022) Density-graded cellular solids: mechanics, fabrication, and applications. Adv Eng Mater (in press)
5. Al-Ketan O, Abu Al-Rub RK (2021) MSLattice: a free software for generating uniform and graded lattices based on triply periodic minimal surfaces. Mater Des Process Commun 3(6):e205
6. Youssef G, Gupta V (2012) Dynamic tensile strength of polyurea. J Mater Res 27:494–499
7. Youssef G, Gupta V (2012) Dynamic response of polyurea subjected to nanosecond rise-time stress waves. Mech Time-Dependent Mater 16(3):317–328

8. Youssef G (2010) Dynamic properties of polyurea (thesis). University of California Los Angeles
9. Huynh NU, Gamez C, Youssef G (2022) Spectro-microscopic characterization of elastomers subjected to laser-induced shock waves. Macromol Mater Eng 307(2):2100506
10. Gupta V, Crum R, Gámez C, Ramirez B, Le N, Youssef G, Citron J, Kim A, Jain A, Misra U (2015) Adhesive and ultrahigh strain rate properties of polyurea under tension, tension/shear, and pressure/shear loadings with applications to multilayer armors. In: Elastomeric polymers with high rate sensitivity: applications in blast, shockwave, and penetration mechanics, pp 71–92
11. Whitten I, Youssef G (2016) The effect of ultraviolet radiation on ultrasonic properties of polyurea. Polym Degrad Stab 123:225107
12. Youssef G, Whitten I (2017) Dynamic properties ultraviolet-exposed polyurea. Mech Time-Depend Mater 21:351–363
13. Ramirez BJ, Kingstedt OT, Crum R, Gamez C, Gupta V (2017) Tailoring the rate-sensitivity of low density polyurea foams through cell wall aperture size. J Appl Phys 121:225107
14. Ramirez BJ, Gupta V (2019) Energy absorption and low velocity impact response of open-cell polyurea foams. J Dyn Behav Mater 5:132–142
15. Ramirez BJ, Gupta V (2019) High tear strength polyurea foams with low compression set and shrinkage properties at elevated temperatures. Int J Mech Sci 150:29–34
16. Reed N, Huynh NU, Rosenow B, Manlulu K, Youssef G (2020) Synthesis and characterization of elastomeric polyurea foam. J Appl Polym Sci 137(26):48839
17. Youssef G, Reed N Scalable manufacturing method of property-tailorable polyurea foam. US Patent, US10899903B2
18. Youssef G, Reed N, Huynh NU, Rosenow B, Manlulu K (2020) Experimentally-validated predictions of impact response of polyurea foams using viscoelasticity based on bulk properties. Mech Mater 148:103432
19. Do S, Huynh NU, Reed N, Shaik AM, Nacy S, Youssef G (2020) Partially-perforated self-reinforced polyurea foams. Appl Sci 10(17):5869
20. Ramirez BJ, Gupta V (2018) Evaluation of novel temperature-stable viscoelastic polyurea foams as helmet liner materials. Mater Des 137:298–304
21. Uddin KZ, Youssef G, Trkov M, Seyyedhosseinzadeh H, Koohbor B (2020) Gradient optimization of multi-layered density-graded foam laminates for footwear material design. J Biomech 109:109950
22. Rusch KC (1970) Energy-absorbing characteristics of foamed polymers. J Appl Polym Sci 14(6):1433–1447
23. Rusch KC (1970) Load-compression behavior of brittle foams. J Appl Polym Sci 14(5):1263–1276
24. Miltz J, Gruenbaum G (1981) Evaluation of cushioning properties of plastic foams from compressive measurements. Polym Eng Sci 21:1010–1014
25. Gruenbaum G, Miltz J (1983) Static versus dynamic evaluation of cushioning properties of plastic foams. J Appl Polym Sci 28:135–143
26. Miltz J, Ramon O (1990) Energy absorption characteristics of polymeric foams used as cushioning materials. Polym Eng Sci 30:129–133
27. Sun Y, Li QM (2018) Dynamic compressive behaviour of cellular materials: a review of phenomenon, mechanism and modelling. Int J Impact Eng 112:74–115
28. Koohbor B, Blourchian A, Uddin KZ, Youssef G (2021) Characterization of energy absorption and strain rate sensitivity of a novel elastomeric polyurea foam. Adv Eng Mater 23(1):2000797
29. Youssef G, Kokash Y, Uddin KZ, Koohbor B (2022) Density-dependent impact-resilience and auxeticity of elastomeric polyurea foams (under review)
30. Koohbor B, Pagliocca N, Youssef G (2021) A multiscale experimental approach to characterize micro-to-macro transition length scale in polymer foams. Mech Mater 161:10406
31. Koumlis S, Lamberson L (2019) Strain rate dependent compressive response of open cell polyurethane foam. Exp Mech 59:1087–1103
32. Pierron F (2010) Identification of Poisson's ratios of standard and auxetic low-density polymeric foams from full-field measurements. J Strain Anal Eng Des 45:233–253
33. Rijensky O, Rittel D (2021) Numerical investigation of polyurea coated aluminum plates under hydrodynamic shocks. Thin-Walled Struct 166:108074
34. Luan S, Kraynik AM, Gaitanaros S (2022) Microscopic and macroscopic instabilities in elastomeric foams. Mech Mater 164:10412
35. Song B, Sanborn B, Lu W-Y (2019) Radial inertia effect on dynamic compressive response of polymeric foam materials. Exp Mech 59:17–27
36. Koohbor B, Ravindran S, Kidane A (2018) Effects of cell-wall instability and local failure on the response of closed-cell polymeric foams subjected to dynamic loading. Mech Mater 116:67–76
37. Roland CM, Twigg JN, Vu Y, Mott PH (2007) High strain rate mechanical behavior of polyurea. Polymer 48:574–578
38. Tripathi M, Parthasaraty S, Kumar D, Chandel P, Sharma P, Roy PK (2020) Strain rate sensitivity of polyurea coatings: viscous and elastic contributions. Polym Test 86:106488
39. Sun Y, Li QM (2015) Effect of entrapped gas on the dynamic compressive behaviour of cellular solids. Int J Solids Struct 63:50–67

Publisher's note Springer Nature remains neutral with regard to jurisdictional claims in published maps and institutional affiliations.